High Rayleigh number convection in a fluid overlaying a porous bed

D. Poulikakos*, A. Bejan†, B. Selimos* and K. R. Blake**

A series of numerical experiments concerning the phenomenon of natural convection in a two-layer composite system heated from below is reported. The composite system consists of a fluid layer bounded from below by a porous bed saturated by the same fluid. The numerical solutions are based on the full equations for time-dependent flow, and document the main features of the flow at Rayleigh numbers several orders of magnitude above critical value. The ranges covered by the numerical solutions are 10^2–10^6 for overall Rayleigh number, 10^{-7}–10^{-4} for Darcy number, and 0.2–1 for the height to length ratio of the composite system.

Keywords: *natural convection, Benard flow, porous media, high Rayleigh numbers*

Introduction

The object of this paper is to report the main conclusions of a numerical study of the phenomenon of natural convection in a fluid layer that is bounded from below by a porous bed saturated with the same fluid. The composite (fluid-bed) layer is heated from below. The large volume of research devoted already to the study of Benard-type convection either in pure fluids[1,2] or in homogeneous porous media[3,4] is the best measure of the importance of this fundamental phenomenon. However, there are numerous environmental and engineering circumstances in which fluid layers and fluid-saturated porous layers are heated together, not separately, from below (eg horizontal layers of fibrous insulation, grain storage installations, post-accident cooling of nuclear reactors). With regard to environmental engineering applications, we note that the thermal circulation in lakes, shallow coastal waters and other reservoirs is influenced by the interaction between the body of water and the water-saturated substrate.

In contrast to the attention received by Benard convection in single layers (fluid layers or fluid-saturated porous layers), the phenomenon that occurs in a composite layer has escaped scrutiny. Exceptions to this pattern are provided by Refs 5–9. In connection with the problem of post-accident cooling of nuclear reactors, Somerton and Catton[5] and Rhee *et al*[9] report the linear stability analysis of natural convection in a bed of heat-generating particles cooled from above by a layer of fluid. The same problem without internal heat generation was formulated analytically by Nield[7,8]; however, the full equations that resulted from linear stability analysis were not solved. Instead, Nield reported closed-form expressions for the critical Rayleigh number for limiting values of the dimensionless parameters that rule the convection phenomenon. Experimental data that are relevant to the critical Rayleigh number range of the same problem as Nield's have been reported by Sun[6].

The present study goes beyond the territory covered by Refs 5–9 and focuses on the high Rayleigh number regime of thermal convection in the composite layer geometry. The numerical experiments described below are based on the full equations for time-dependent flow and offer a view of the phenomenon at Rayleigh numbers that are several orders of magnitude higher than critical value.

Mathematical formulation

Consider the two-layer configuration sketched in Fig 1. A horizontal fluid layer of depth h floats on top of a porous bed of thickness h_p. The overall thickness of the composite layer is denoted by H. The two horizontal walls that bound the system from above and from below are assumed impermeable and isothermal, with temperatures T_C and T_H, respectively. It is assumed further that the system is potentially unstable: in other words, that $T_H > T_C$ and that the fluid residing in the h-deep upper layer and in the pores of the substrate expands upon heating.

The focus of this study is on the convection regime, that is, on situations characterized by fluid flow and convective heat transfer in the two-layer configuration. Unable to study the flow numerically in a domain that extends to infinity in the horizontal direction, we select for analysis a section of finite length L and assume that the vertical walls located at $x=0$ and $x=L$ are impermeable and adiabatic. It is well known that the finite length L will have an effect on the computed field only when it is comparable to (and, certainly, when it would be smaller than) the horizontal length scale of each two-dimensional roll of the Benard flow. In a domain where L is fixed, the rolls become thinner and multiply as the bottom-top temperature difference increases. For example, if the HxL domain contains only fluid-saturated porous material, the horizontal thickness of each roll decreases as $HRa_H^{-1/2}$ since the Darcy-Rayleigh number $Ra_H = Kg\beta(T_H - T_C)/\alpha\nu$ increases[10]. It follows that in the high Rayleigh number

*Department of Mechanical Engineering, University of Illinois at Chicago, Box 4348, Chicago, IL 60680, USA
†Department of Mechanical Engineering and Materials Science, Duke University, Durham, NC 27706, USA
**Creare Inc., Etna Road, PO Box 71, Hanover, NH 03755, USA

regime the overall length L ceases to influence the overall characteristics of the flow, since it is large enough to accommodate an increasing number of rolls whose individual geometry is independent of L.

The fluid layer ($h_p < y \leq H$)

The conservation of mass, momentum and energy in the system of Fig 1 is accounted for by two different sets of partial differential equations, one set for each layer. For the upper fluid layer we invoke the Navier–Stokes–Boussinesq equations:

$$\nabla \cdot \boldsymbol{u} = 0 \tag{1}$$

$$\frac{\partial \boldsymbol{u}}{\partial t} + \boldsymbol{u} \cdot \nabla \boldsymbol{u} = -\frac{1}{\rho_0} \nabla P + \nu \nabla^2 \boldsymbol{u} - [1 - \beta(T - T_0)]\boldsymbol{g} \tag{2}$$

$$\frac{\partial T}{\partial t} + \boldsymbol{u} \cdot \nabla T = \alpha \nabla^2 T \tag{3}$$

where x and y refer to the cartesian system of coordinates in Fig 1, and where $\boldsymbol{u}(u,v)$, T, P, ν, α, β and ρ_0 are the velocity vector and its components, the temperature, pressure, kinematic viscosity, thermal diffusivity, coefficient of thermal expansion, and density (subscript 0 denotes a reference state). The $\boldsymbol{g}$ vector is the gravitational acceleration pointing in the negative y-direction. In accordance with the Boussinesq approximation the fluid density is assumed constant in every term except in the buoyancy term of the momentum equation where its dependence on temperature is assumed linear,

$$\rho = \rho_0[1 - \beta(T - T_0)] \tag{4}$$

The numerical experiments described below, under 'Numerical procedure', are based on a dimensionless version of Eqs (1)–(3). Introducing the new variables

$$(x^*, y^*) = (x,y)/H,\ (u^*, v^*) = (u,v)/(\nu/H)$$
$$t^* = t/(H^2/\nu),\ T^* = (T - T_C)/(T_H - T_C) \tag{5}$$

and the dimensionless streamfunction (ψ^*) and vorticity (ω^*),

$$\frac{\partial \psi^*}{\partial y^*} = u^*, \qquad \frac{\partial \psi^*}{\partial x^*} = -v^* \tag{6,7}$$

$$\omega^* = -\nabla^2 \psi^* \tag{8}$$

the dimensionless equations become

$$\frac{\partial \omega^*}{\partial t^*} + \nabla \cdot \boldsymbol{u}^* \omega^* = \nabla^2 \omega^* + \frac{Ra}{Pr} \frac{\partial T^*}{\partial x^*} \tag{9}$$

$$\frac{\partial T^*}{\partial t^*} + \nabla \cdot \boldsymbol{u} T^* = \frac{1}{Pr} \nabla^2 T^* \tag{10}$$

where Ra and Pr are the overall Rayleigh number and the Prandtl number,

$$Ra = \frac{g\beta H^3 (T_H - T_C)}{\nu \alpha} \tag{11}$$

$$Pr = \frac{\nu}{\alpha} \tag{12}$$

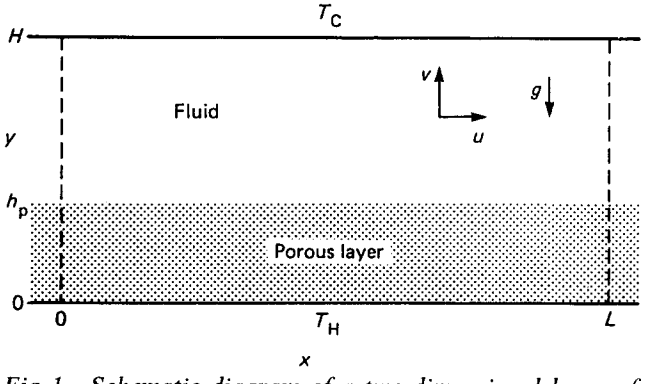

Fig 1 Schematic diagram of a two-dimensional layer of fluid floating on top of a porous bed heated from below

The porous layer ($0 \leq y < h_p$)

For the fluid-saturated porous bed we use the homogeneous porous medium model coupled with the Darcy flow model. This description is well known[3,4]; in

Notation

Da	Darcy number, K/H^2
g	Gravitational acceleration
h	Thickness of fluid layer
h_p	Thickness of porous layer
H	Overall thickness of composite layer
k	Thermal conductivity
K	Permeability
L	Horizontal length
Nu	Nusselt number, $QH/kL(T_H - T_C)$
P	Pressure
Pr	Prandtl number, ν/α
Q	Overall heat transfer rate
Ra	Rayleight number, $g\beta H^3(T_H - T_C)/\alpha\nu$
t	Time
T	Temperature
T_C	Cold wall temperature
T_H	Hot wall temperature
u,v	Velocity components (Fig 1)
x,y	Cartesian coordinates (Fig 1)
α	Thermal diffusivity of fluid
α_p	Thermal diffusivity of fluid-saturated porous bed
$\tilde{\alpha}$	Coefficient in Bevers and Joseph's matching condition (Eq (21))
β	Coefficient of thermal expansion
γ	Relaxation parameter
ν	Kinematic viscosity
ρ	Density
ψ	Streamfunction
ω	Vorticity

Subscripts

0	Reference property
+	Quantity evaluated on the fluid side of the fluid-bed interface
−	Quantity evaluated on the porous bed side of the fluid-bed interface

Superscripts

*	Dimensionless variable

the interest of brevity, we list only the dimensionless set of governing equations corresponding to the lower layer in Fig 1:

$$\nabla^2\psi^* = -\left(\frac{RaDa}{Pr}\right)\left(\frac{\alpha}{\alpha_p}\right)\frac{\partial T^*}{\partial x^*} \tag{13}$$

$$\frac{\partial T^*}{\partial t^*} + \nabla\cdot\boldsymbol{u}^* T^* = \left(\frac{\alpha_p}{\alpha}\right)\left(\frac{1}{Pr}\right)\nabla^2 T^* \tag{14}$$

The streamfunction ψ^* and velocity vector $\boldsymbol{u}^*$ have been defined already in Eqs (5)–(7); however, in the lower layer discussed here, u and v represent the volume-averaged velocity components of the flow permeating through the porous bed. The remaining dimensionless variables, x^*, y^*, t^*, T^*, Ra and Pr, have the same meaning as in Eqs (5), (11) and (12). However, in accordance with the homogeneous porous medium model, the temperature T represents the local equilibrium temperature of the fluid and solid phases in the porous bed. New parameters in Eqs (13) and (14) are the thermal diffusivity of the porous medium, α_p, defined as the thermal conductivity of the porous medium saturated with fluid divided by the specific heat capacity of the fluid phase, and the Darcy number

$$Da = \frac{K}{H^2} \tag{15}$$

where K is the permeability of the porous medium in the Darcy flow regime. As shown below, in the discussion of the results, the Darcy numbers of the cases selected for numerical analysis were sufficiently small to assure the validity of the Darcy flow model.

Boundary and initial conditions

The problem statement is completed by specifying appropriate boundary conditions around the rectangular domain of size HxL and along the horizontal interface ($y = h_p$) between the fluid layer and the porous bed. In the dimensionless notation defined already, the boundary conditions along the periphery of the system are

$$\psi^* = 0, \quad T^* = 1 \quad \text{at} \quad y^* = 0 \tag{16}$$

$$\psi^* = \frac{\partial \psi^*}{\partial y^*} = T^* = 0 \quad \text{at} \quad y^* = 1 \tag{17}$$

$$\psi^* = \frac{\partial T^*}{\partial x^*} = 0 \quad \text{at} \quad x^* = 0,\ L/H \quad \text{and} \quad 0 \leqslant y^* < h_p/H \tag{18}$$

$$\psi^* = \omega^* = \frac{\partial T^*}{\partial x^*} = 0 \quad \text{at} \quad x^* = 0,\ L/H \quad \text{and} \quad h_p/H < y^* \leqslant 1 \tag{19}$$

It is worth noting here the difference between Darcy flow and Navier–Stokes flow, in that the no-slip condition cannot be satisfied along the bottom wall, Eq (16), and along the lower portions of the lateral walls, Eq (18). Note further the zero vorticity conditions ($\omega^* = 0$) used along the upper portions of the lateral walls, Eqs (19): this condition is invoked in order to minimize the inhibitive influence that the lateral walls might have on the flow that might exist in a much wider domain. The effect of this particular boundary condition was studied in one series of numerical experiments in which the $\omega^* = 0$ condition was replaced with the no-slip condition $\partial\psi^*/\partial x^* = 0$ in Eqs (19) (see discussion, below).

The matching of the fluid and porous bed temperatures across the horizontal interface is straightforward: we simply require that T^* varies continuously across $y^* = h_p/H$. However, the matching conditions for the velocity field deserve careful examination. The difficulty stems from the fact that on the fluid side of the interface, $y^* = (h_p/H)_+$, the vorticity-streamfunction equations (8) and (9) admit two boundary conditions, whereas on the porous side of the same interface, $y^* = (h_p/H)_-$, the Darcy flow model, Eq (13), permits the specification of only one boundary condition. In order to overcome this difficulty we used the matching conditions proposed by Beavers and Joseph[11]

$$v_+^* = v_-^* \quad \text{at} \quad y^* = h_p/H \tag{20}$$

$$\left(\frac{\partial u^*}{\partial y^*}\right)_+ = \tilde{\alpha} Da^{-1/2}(u_+^* - u_-^*) \tag{21}$$

where the subscripts + and − indicate that the respective quantities are calculated while approaching the interface from above and from below. The first matching condition, Eq (20), states that the interface is permeable and that the vertical velocity component v^* varies continuously across the interface. The second condition, Eq (21), relates the shear experienced by the fluid that flows along the permeable surface, $(\partial u^*/\partial y^*)_+$, to the velocity difference between the tangential velocity of the fluid, u_+^*, and the volume-averaged tangential velocity present in the porous bed, u_-^*. The Beavers–Joseph constant $\tilde{\alpha}$ is dimensionless and of order unity. It is worth keeping in mind that the choice of matching conditions at the fluid–bed interface depends on the model used to describe the flow through the porous medium[5,12,13], and that the Beavers–Joseph conditions perform quite well when used in conjunction with the Darcy flow model[11,14], that is, in conjunction with the porous medium model adopted in this study.

The numerical experiments described below consist of following the time evolution of the flow and temperature fields starting from the initial condition of motionless isothermal fluid throughout the H-deep system,

$$\psi^* = 0, \quad T^* = 1 \quad \text{at} \quad t^* = 0 \tag{22}$$

In accordance with Eqs (16) and (17), the temperature of the top wall is lowered suddenly to $T^* = 0$, and the bottom wall temperature is kept at $T^* = 1$ throughout the duration of the experiment, $t^* > 0$.

Numerical procedure

The dimensionless equations (8)–(10), (13) and (14) were discretized using the control volume formulation discussed by Patankar[15]. The rectangular domain HxL was covered by n vertical and m horizontal and equidistant grid lines. The grid points created at the intersection of interior grid lines were surrounded by square control volumes in such a way that each control volume contained a single grid point located in its geometric centre. It was found that a total of $n-2=22$ control volumes counted in the vertical direction (including the two control volumes at the top and bottom boundaries) constitute an acceptable trade-off between

accuracy and computation time (Table 1). The number of control volumes needed in the horizontal direction depended on the geometric slenderness ratio H/L, for example, in a domain with $H/L=1/2$ we used $m-2=42$ control volumes in the horizontal direction. In most of the numerical runs summarized in Table 1, the time step that was used and yielded convergence was $\Delta t^*=0.1$.

The power law scheme, introduced, tested and recommended by Patankar[15], was employed to calculate the vorticity from Eq (9), the fluid layer temperature from Eq (10), and the porous layer temperature from Eq (14). The fluid layer streamfunction was obtained using Eq (8); the streamfunction values for the porous layer were obtained in the same way from Eq (13). In most cases, underrelaxation was necessary to insure convergence: $\gamma=0.8$ is a typical value of the underrelaxation parameter used in this study.

The numerical integration started from the top wall and proceeded using the fluid layer equations until reaching the grid points situated immediately above the horizontal interface $y=h_p$. Next, the discretized form of the interface matching conditions (20) and (21) was used to advance the solution from the lowest grid points of the fluid layer to the uppermost grid points of the porous layer. Note that no grid points were positioned along the interface. Following this procedure of crossing the interface, the discretized form of the porous medium equations was used to advance the solution down to the bottom wall. After sweeping all the grid points of the HxL domain, the time t^* was increased by one time step Δt^*. The entire procedure was repeated until steady state was reached and the temperature and flow fields satisfied the criterion

$$\frac{\sum_{i=1}^{m}\sum_{j=1}^{n}|\phi_{i,j}^{r+1}-\phi_{i,j}^{r}|}{\sum_{i=1}^{m}\sum_{j=1}^{n}|\phi_{i,j}^{r+1}|}<10^{-4} \tag{23}$$

where ϕ stands for T^* or ψ^* and r denotes the number of time steps counted from the beginning of the time-dependent solution.

Additional calculations were carried out in order to evaluate the effect of fluid motion on the overall heat transfer rate between the two horizontal walls that confine the composite layer,

$$Q=-k\int_0^L\left(\frac{\partial T}{\partial y}\right)_{y=0}\mathrm{d}x \tag{24}$$

The overall heat transfer rate can be expressed in dimensionless form as the conduction-referenced Nusselt number

$$Nu=\frac{Q}{kL(T_H-T_C)/H} \tag{25}$$

that, in terms of the dimensionless variables of the present formulation, becomes

$$Nu=-\frac{H}{L}\int_0^{L/H}\left(\frac{\partial T^*}{\partial y^*}\right)_{y^*=0}\mathrm{d}x^* \tag{26}$$

A Nusselt number expression analogous to Eq (26) can be written by integrating the heat flux along the top wall ($y^*=1$). This second Nu calculation was carried out and the results were found to be in good agreement with the values obtained on the basis of Eq (26).

The effect of grid fineness on the flow and heat transfer predictions is documented in the fourth group of runs assembled in Table 1, ie for the case of one of the highest Rayleigh numbers considered in this study ($Ra=10^5$). As the grid changes from 22×42 to 32×62, the overall Nusselt number increases by 4.5%: keeping in mind that the Nu change becomes considerably smaller at lower Ra values, the grids chosen for this study were all as fine as the 22×42 grid used for $H/L=1/2$. The effect of grid fineness on the streamfunction maximum ψ^*_{max} is similar to the effect on Nu. Furthermore, given the thickness of the line that was used in drawing the streamline patterns of Fig 2, there would be no visual difference between the patterns calculated with 22×42 and 32×62 grids. For these reasons, we used the fineness of the 22×42 grid (when $H/L=1/2$) as a good trade-off between high accuracy and high computation cost.

Table 1 Summary of numerical results

H/L	Ra	Nu	γ	Da	$\tilde{\alpha}$	ψ^*_{max}	Number of control volumes
1/2	10^2	1	0.8	10^{-6}	1	10^{-3}	22×42
	10^3	1.15				0.287	
	10^4	2.70				4.12	
	10^5	5.285				12.51	
	10^6	12.35				45.161	
1/2	10^5	5.814	0.8	10^{-6}	0.1	12.45	22×42
		5.82			0.5	12.48	
		5.83			5	12.53	
		5.832			10	12.55	
1/2	10^5	5.83	0.8	10^{-4}	1	12.52	22×42
		5.82		10^{-5}		12.51	
		5.82		10^{-7}		12.51	
1/2	10^5	4.36	0.8	10^{-6}	1	7.99	12×22
		5.825				12.51	22×42
		6.1				13.4	32×62
1	10^5	2.795	0.8	10^{-6}	1	2.13	22×22
2/3		4.2				5.74	22×32
2/5		8.401				29.83	22×52
1/3		9.04				46.88	22×62
2/7		9.36				62.82	22×72
1/4		9.4				70.52	22×82
2/9		9.6				83.03	22×92
1/5		10.1				103.0	22×100
1/4	10^5	9.4	0.8	10^{-6}	1	70.52	22×82
	5×10^5	9.9				76.74	
	10^6	11.75				84.38	

Discussion of results

Relative to the classical two-dimensional Benard problem, which depends on three dimensionless groups (Ra, Pr and H/L), the phenomenon of natural convection in the two-layer geometry of Fig 1 depends on four additional parameters (Da, h_p/H, α_p/α and the Beavers–Joseph parameter $\tilde{\alpha}$). In the face of so many parameters that might be able to change the complexion of the flow, we made a special effort to analyse the effect of one

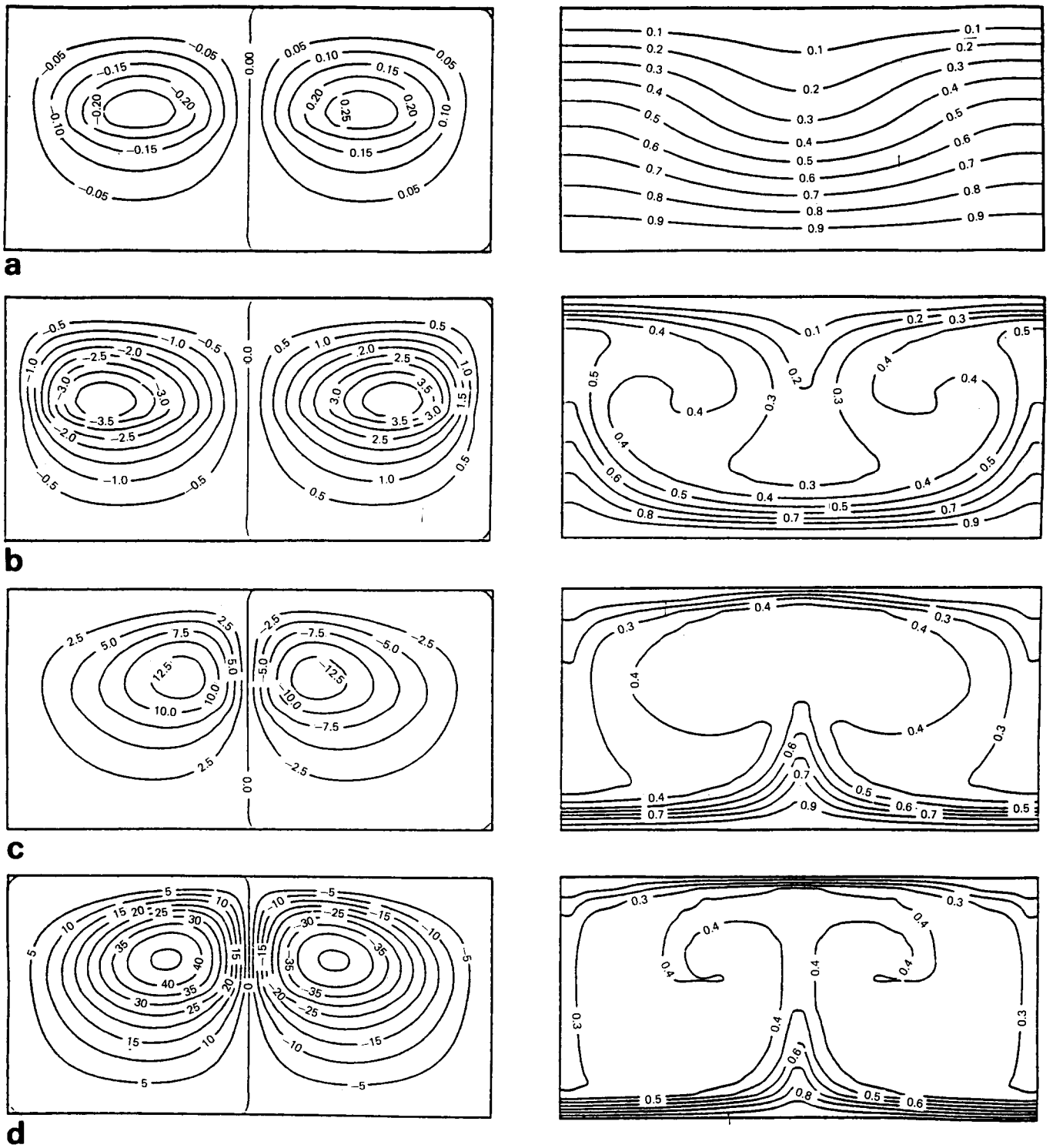

Fig 2 Patterns of streamlines and isotherms showing the effect of increasing the Rayleigh number (H/L = *1/2*, Da = 10^{-6}, $\tilde{\alpha}$ = *1*): (*a*) Ra = 10^3; (*b*) Ra = 10^4; (*c*) Ra = 10^5; (*d*) Ra = 10^6

parameter at a time and place more emphasis on those parameters that distinguish the present problem from the traditional Benard flow in a homogeneous medium.

The relevant overall parameters of the numerical experiments performed in this study are summarized in Table 1. Throughout these experiments the Prandtl number, the thermal diffusivity ratio and the position of the fluid–bed interface were held fixed,

$$Pr = 7, \quad \frac{\alpha_p}{\alpha} = 1, \quad \frac{h_p}{H} = 0.5 \tag{27}$$

We selected these particular values in order to facilitate the job of comparing the present results against future laboratory simulations (the most frequently used laboratory fluid is water, and the porous bed usually has a high enough porosity so that $\alpha_p \approx \alpha$).

The message of the numerical results assembled in Table 1 becomes clearer if we first take a look at the kind of flow and temperature patterns that rule the convective steady state in the rectangular domain *HxL*. Fig 2 shows a sequence of four solutions, where all the dimensionless parameters are held fixed except the Rayleigh number.

From Fig 2(a) to 2(d) the Rayleigh number increases by one order of magnitude at a time from 10^3 to 10^6. To the eye that is already acquainted with the main features of Benard convection in homogeneous layers, this sequence of flow patterns reveals both expected and unexpected characteristics. Expected is the symmetric cellular flow whose intensity increases with the Rayleigh number. However, in the *Ra* range 10^3–10^6 the number of two-dimensional rolls does not change.

One new feature of the patterns of Fig 2 is the presence of kinks in the streamlines that cross the plane of the fluid–bed interface. These kinks appear to be less visible as *Ra* increases (compare, for example, Fig 2(a) with Fig 2(d)). Another way of stating the same observation is to say that while decreasing the Rayleigh number and keeping everything else constant, the flow is progressively forced out of the porous bed.

Another interesting characteristic that was revealed consistently by the numerical solutions is the flow reversal that is observed as *Ra* increases. In the sequence displayed in Figs 2(a)–2(d), the sense of rotation of the left roll changes from clockwise in Figs 2(a) and 2(b) to counterclockwise in Figs 2(c) and 2(d). (Note that at the same time the sense of the right roll changes from counterclockwise to clockwise: the flow symmetry about the vertical midplane is preserved, as is required by the boundary conditions (18) and (19).) Additional runs using different aspect ratios (*H/L*), Beavers–Joseph factors ($\tilde{\alpha}$) and relaxation factors (γ) showed that the flow reversal does not disappear. The flow reversal behaviour is also insensitive to changing the zero vorticity boundary condition in Eqs (19): this finding is discussed below in connection with the solutions for shallower domains (Fig 4).

Related to the numerical solution displayed in Fig 2(c), the next two graphs show the conclusions of investigating the effect of Darcy number and Beavers–Joseph factor (Figs 3(a) and 3(b)). It is clear that in the range covered by these tests the effect of changes in *Da* and $\tilde{\alpha}$ is insignificant. It is important to note that in the present study the Darcy number values have been restricted to the

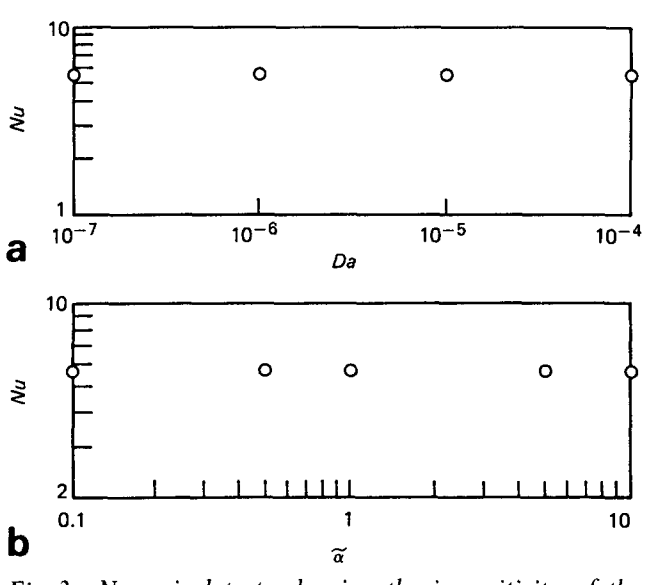

Fig 3 Numerical tests showing the insensitivity of the solution to changes in Darcy number and in the Beavers–Joseph parameter: (a) Nu *versus* Da (Ra = 10^5, H/L = 1/2, $\tilde{\alpha}$ = 1); *(b)* Nu *versus* $\tilde{\alpha}$ (Ra = 10^5, H/L = 1/2, Da = 10^{-6})

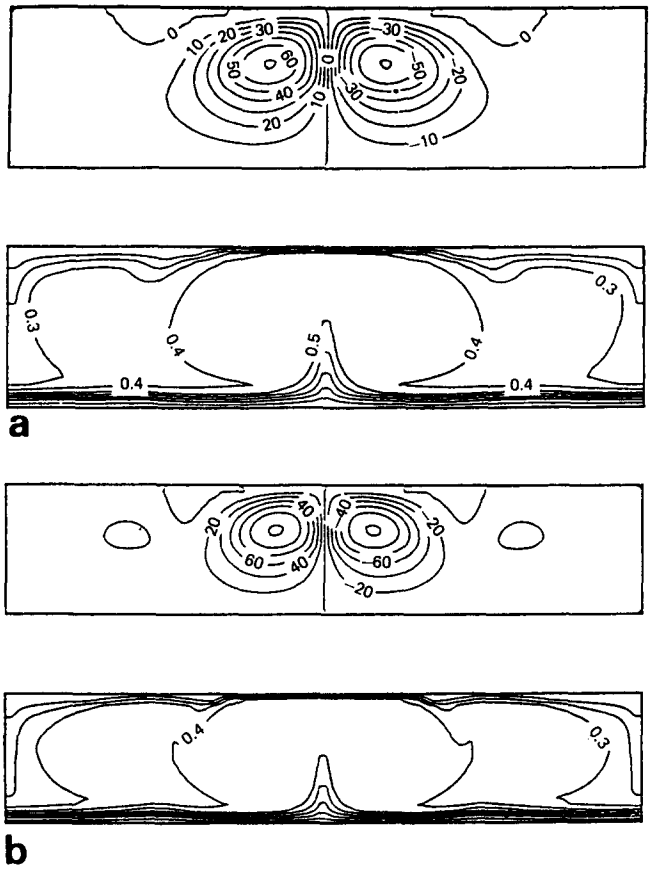

Fig 4 Patterns of streamlines and isotherms showing the effect of decreasing the overall geometric aspect ratio (Ra = 10^5, Da = 10^{-6}, $\tilde{\alpha}$ = 1)

10^{-7}–10^{-4} range in order not to violate the Darcy flow model, Eq (13). In the earliest numerical study of natural convection in a rectangular enclosure filled with porous medium and heated from the side, Chan *et al*[16] showed that the Darcy flow model is adequate if *Da* is less than 10^{-3}. The same issue, ie the goodness of the Darcy model versus the Brinkman-extended Darcy model (which allows the imposition of the no-slip boundary condition along a solid wall), was considered in depth by a number of more recent studies[17–20]. For example, in terms of the present notation, Tong and Subramanian[20] found that the Darcy flow model applies to natural convection in an *H*-tall porous layer heated from the side if

$$\frac{Kg\beta\Delta T}{\alpha\nu}Da < 10^{-4} \tag{28}$$

where ΔT is the side-to-side temperature difference. Noting that in Darcy flow the maximum velocity scale in layers heated from the side[21] is the same as in *H*-deep porous layers heated from below[10] (namely $Kg\beta\Delta T/\nu$), the validity criterion (28) can be used in the present study with reference to the porous bed section of Fig 1. Recalling the definition of overall Rayleigh number *Ra*, Eq (11), the condition (28) translates into

$$Da < 10^{-2}Ra^{-1/2} \tag{29}$$

In the case of $Ra = 10^5$, Fig 3, the above criterion yields $Da < 0.3 \times 10^{-4}$ as the upper limit of the Darcy number range in which the present numerical experiments are justified. This scaling conclusion is consistent with the

Darcy number order of magnitude considered in the present study.

Taken together, Figs 2(c), 4(a) and 4(b) illustrate the effect of decreasing the aspect ratio H/L while keeping the overall Rayleigh number constant. As one reads this sequence of flow and temperature patterns, every dimension of the problem remains fixed while only the horizontal dimension L increases. We see that as the aspect ratio decreases from 1/2 to 1/5 the number of two-dimensional cells does not change. The crowding of the flow around the vertical mid-plane of the HxL domain appears to be insensitive to the widening of the flow region. At the same time, however, the circulation becomes more intense. Fig 4(b) shows the beginning of the process of cell multiplication, which is expected as H/L decreases. The phenomenon of discrete cell multiplication is amply documented in two recent studies of Benard convection in a pure fluid layer[22] and a pure porous layer[23], which used the same numerical scheme as the present study.

In order to verify that the artificial imposition of lateral boundaries does not influence appreciably this behaviour, we replaced the $\omega^*=0$ condition of Eq (19) with that of no-slip ($\partial\psi^*/\partial x^*=0$). We found that this change does not affect the overall structure of the flow. In going from zero vorticity to zero vertical velocity along the upper sections of the two lateral walls the only visible change appears to be the roughly 15% decrease of the streamfunction maximum. The corresponding change in overall Nusselt number is smaller than 15% (this behaviour is consistent with the relative effect of grid fineness on ψ^*_{max} and Nu (Table 1)).

An overall view of the heat transfer characteristics of the two-layer system is provided by Fig 5. The transition from the conduction regime to convection occurs rather abruptly in the Ra range 500–600. The high Ra end of this transition is illustrated by the sequence presented in Fig 2. At Rayleigh numbers that are at least one order of magnitude above critical value, the overall Nusselt number data define the power law curve

$$Nu \simeq 0.129 Ra^{0.33}, \quad (H/L = 1/2) \tag{30}$$

The 0.33 exponent of Ra matches the value 1/3 recommended by the scales of Benard convection in a pure fluid[10].

The effect of varying the aspect ratio is further illustrated in Fig 6 by plotting the overall Nusselt number as H/L changes in relatively small steps from 1/5 to 1. In the direction of small aspect ratios the Nusselt number is relatively insensitive as the cells multiply stepwise to fill the space created by increasing L. In the opposite

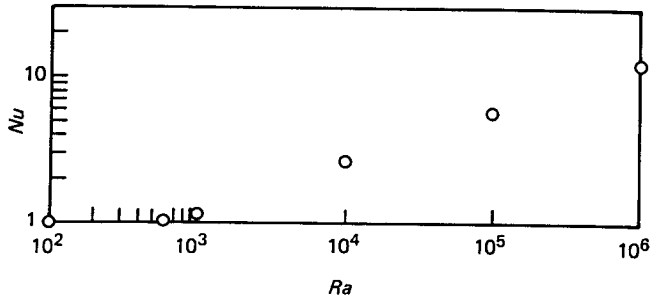

Fig 5 The relationship between the Nusselt number and the Rayleigh number in the convection regime (H/L = *1/2*, Da = 10^{-6}, $\tilde{\alpha}=1$)

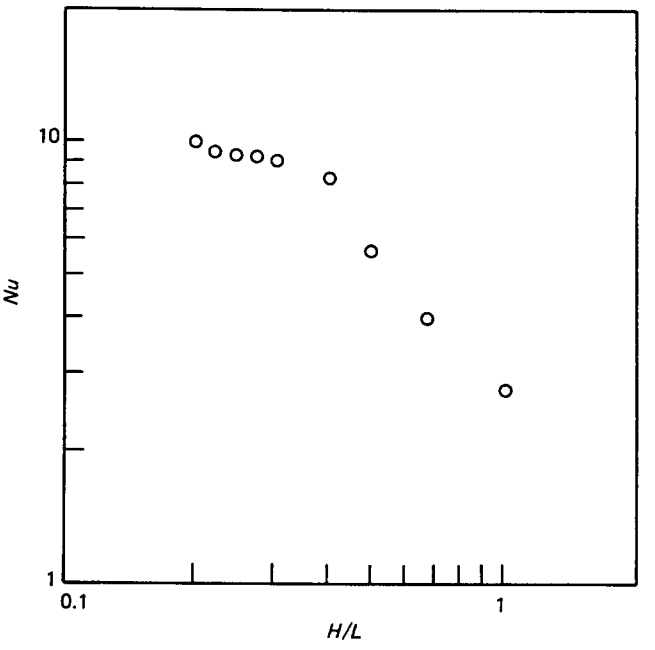

Fig 6 The effect of the overall geometric aspect ratio on the Nusselt number (Ra = 10^5, Da = 10^{-6}, $\tilde{\alpha}=1$)

direction, however, there is a definite decrease in the slope of the Nu–H/L curve as H/L increases above approximately 0.4. This behaviour suggests that in the range $H/L>0.4$ the lateral walls are close enough to interfere with (and slow down) the circulation.

Conclusion

In this study we relied on transient numerical experiments to illustrate the occurrence of convection in a fluid layer which floats on top of a fluid-saturated porous medium that is heated from below. These numerical simulations provide for the first time a view of the main features of the flow in the convective regime, ie at Rayleigh numbers considerably larger than the critical value needed for the onset of convection.

Although many of the flow characteristics confirm the expectations based on previous knowledge of Benard convection in pure fluids and homogeneous porous media, the numerical solutions obtained for the composite layer configuration of Fig 1 reveal a number of special features that deserve future attention. Among these, the effect of changing the (porous bed)–(pure fluid) interface model, Eqs (20) and (21), requires further numerical study and comparison with laboratory measurements. The present solutions are all based on transient numerical experiments that evolve to a steady state: we did not attempt to solve the steady state problem directly (ie by dropping the $\partial/\partial t$ terms from the governing equations).

Acknowledgement

D. Poulikakos and B. Selimos gratefully acknowledge the financial support provided by NSF Grant No ENG-84-51144. A. Bejan acknowledges the support received through NSF Grant No MEA-84-21250.

References

1. **Chandrasekhar S.** *Hydrodynamic and Hydromagnetic Stability, Clarendon Press, Oxford, 1961*

2. **Drazin P. G. and Reid W. H.** *Hydrodynamic Stability, Cambridge University Press, 1981*
3. **Cheng P.** Heat transfer in geothermal systems. *Advances in Heat Transfer, 1979,* **14**, *1–105*
4. **Combarnous M. A.** Natural convection in porous media and geothermal systems. *Proc. 6th Int. Heat Transfer Conf., 1978, Vol 6, 45–59*
5. **Somerton C. W. and Catton I.** On the thermal instability of superposed porous and fluid layers. *J. Heat Transfer, 1982,* **104**, *160–165*
6. **Sun W. J.** Convective instabilities in superposed porous and free layers, *Ph.D. Thesis, University of Minnesota, Minneapolis, 1973*
7. **Nield D. A.** Onset of convection in a fluid layer overlaying a layer of porous medium. *J. Fluid Mech., 1977,* **81**, *513–522*
8. **Nield D. A.** The boundary correction of the Rayleigh–Darcy problem: limitations of the Brinkman equation. *J. Fluid Mech., 1983,* **128**, *37–46*
9. **Rhee S. J., Dhir V. K. and Catton I.** Natural convection heat transfer in beds of inductively heated particles. *J. Heat Transfer, 1978,* **100**, *78–85*
10. **Bejan A.** *Convection Heat Transfer, Wiley, New York, 1984, 413*
11. **Beavers G. S. and Joseph D. D.** Boundary conditions at a naturally permeable wall. *J. Fluid Mech., 1967,* **30**, *197–207*
12. **Neale G. and Nader W.** Practical significance of a Brinkman's extension of Darcy's law: coupled parallel flows within a channel and a bounding porous medium. *Canadian J. Chem. Eng., 1974,* **52**, *475–478*
13. **Ross S. M.** Theoretical model of the boundary condition at a fluid–porous interface. *AIChE J., 1983,* **29**, *840–846*
14. **Sparrow E. M., Beavers G. S., Chen T. S. and Lloyd J. R.** Breakdown of the laminar flow regime in permeable walled ducts, *J. Appl. Mech. 1973,* **40**, *337–342*
15. **Patankar S. V.** *Numerical Heat Transfer and Fluid Flow, Hemisphere, Washington, DC, 1980*
16. **Chan B. K. C., Ivey C. M. and Barry J. M.** Natural convection in enclosed porous media with rectangular boundaries. *J. Heat Transfer, 1970,* **92**, *21–27*
17. **Vafai K. and Tien C. L.** Boundary and inertia effects on flow and heat transfer in porous media. *Int. J. Heat Mass Transfer, 1981,* **24**, *195–203*
18. **Vafai K. and Tien C. L.** Boundary and inertia effects on convective mass transfer in porous media. *Int. J. Heat Mass Transfer, 1982,* **25**, *1183–1190*
19. **Vafai K.** Convective flow and heat transfer in variable porosity media. *J. Fluid Mech., 1984,* **147**, *233–259*
20. **Tong T. W. and Subramanian E.** A boundary layer analysis for natural convection in vertical porous enclosures—use of the Brinkman-extended Darcy model. *Int. J. Heat Mass Transfer, 1985,* **28**, *563–571*
21. **Poulikakos D. and Bejan A.** Unsteady natural convection in a porous layer. *Phys. Fluids, 1983,* **26**, *1183–1191*
22. **Blake K. R., Poulikakos D. and Bejan A.** Natural convection near 4°C in a horizontal water layer heated from below. *Phys. Fluids, 1984,* **27**(*1*), *2608–2616*
23. **Blake K. R., Bejan A. and Poulikakos D.** Natural convection near 4°C in a water saturated porous layer heated from below. *Int. J. Heat Mass Transfer, 1984,* **27**, *2355–2364*

Books received

Fluid Mechanics and Transfer Process, *J. M. Kay and R. M. Nedderman*, £45 h/c ($69.00), £17.50 p/b ($29.95), pp 602, Cambridge University Press

Finite Elements in Fluids, *eds R. H. Gallagher, G. Carey, J. T. Oden and O. C. Zienkiewicz*, £42.40, pp 358, John Wiley and Sons

Thermodynamics and Fluid Mechanics of Turbomachinery Vol I and II, *eds A. S. Ucer, P. Stow and Ch. Hirsch*, Dfl. 395,000, US$148.00, £109.50, pp 598, and 495, Martinus Nijhoff (Price is for both volumes)

The Exergy Method of Thermal Plant Analysis, *T. J. Kotas*, £45.00, pp 296, Butterworth Scientific Ltd

Heat Transfer of a Cylinder in Crossflow, A. Žukauskas and J. Žiugžda, *ed G. F. Hewitt*, DM 218, pp 208, Springer GmbH and Co

Fundamentals of Hot Wire Anemometry, *Charles G. Lomas*, £35.00, US$52.50, pp 211, Cambridge University Press

Developments in Boundary Element Methods—4, *eds P. K. Banerjee, and J. O. Watson*, £42.00, pp 346, Elsevier Applied Science Publishers Ltd

Heat and Mass Transfer in Fixed and Fluidized Beds, *eds W. P. M. van Swaaij and N. H. Afjan*, DM 328, pp 732, Springer Verlag GmbH

Heat Exchanger and Pressure Vessel Technology, *J. P. Gupta*, DM 138, pp 607, Springer Verlag GmbH

Stability of Parallel Gas Flows, *B. K. Shivamaggi*, £20, pp 169, John Wiley and Sons

Turbulence and Random Processes in Fluid Mechanics, *M. T. Landahl, E. Mollo-Christenson*, £20, $34.50, pp 154, Cambridge University Press

Forthcoming articles

Axisymmetric free convection boundary layer flow of water at 4°C past slender bodies
R. S. R. Gorla and R. A. Stratman

Determination of principal characteristics of turbulent swirling flow along annuli. Part III Numerical analysis
T. S. M. Morsi and B. R. Clayton

Transition to time-dependent free convection in inclined air layer
J. F. Pignatel and J. F. Marcillat

Effect of drainage discs on the condensing heat transfer performance of vertical fluted tubes
H. Gokce, C. Ozgen and T. G. Somer

Effect of temperature gradient locally applied on a long horizontal cavity
G. P. Extremet and B. Roux

On the three exponents of the isentropic change of the refrigerant R22
D. A. Kouremenos and X. K. Kakatsios